Experimental Evaluation of Higher Order Stability Zones Using a Digitally Operated Quadrupole Mass Filter

Sumeet Chakravorty[1], Elizabeth Groetsema[1], Fatima Olayemi Obe[1], Adam P. Huntley[1], Gordon A. Anderson[2], *Brian H. Clowers[1], and Peter T. A. Reilly[1]

[1] Department of Chemistry, Washington State University, Pullman, WA 99164
[2] GAA Custom Electronics LLC, Kennewick, WA 99338

*Corresponding Author: brian.clowers@wsu.edu

Abstract

Recent improvements to the comparison-based method of digital waveform generation increased the reproducibility of the waveforms so that the higher-order Mathieu stability zones can be accessed reliably. Digitally driven quadrupole mass filters access these zones using a fixed AC voltage and rectangular waveforms that are defined by a duty cycle. In this context, the duty cycle is the fraction of the waveform period where the waveform remains in the high state. Because digitally driven quadrupoles navigate stability using a duty cycle, there is no need to apply a resolving DC offset between electrode pairs. Accessing the higher stability zones using a conventional resonantly-tuned RF requires the use of thousands of AC and DC voltages making the mode of operation less accessible with these devices. Stability zones higher than (1,1) and (2,1) have theoretical resolving powers that are on the order 1,140 and 3,447 at FWHM which drives efforts to practically access these operational conditions. Accessing these zones digitally requires the use of extremely precise waveforms. In a previous effort, waveform generation produced waveforms to reliably access the (1,1) and (2,1) zones without impacting performance. However, recent work found more improvement was needed to reliably access neighboring higher stability zones. Derived from that work, it was determined that a waveform resolution of ~10 ppm or less was needed to reliably access the (3,1) and (3,2) zones. The present work utilized digital waveforms that achieve this level of precision to experimentally access and characterize attributes of the (3,1) and (3,2) zones. This work dives into the investigation of different beam energies to overcome the destabilizing fringing fields, improve transmission, and their overall effect on the experimental resolving power and signal-to-noise. In addition, the AC voltage of the driving RF was varied to understand the effects on the initial ion beam energy that is needed to achieve balanced separation and how the overall signal-to-noise is affected. Lastly, an assessment was made on the effects of the temporal parameters of a digital mass scan on peak sensitivity, peak fidelity, and overall duration for a scan.

Introduction

The conventional sine-driven quadrupole is commonplace and featured in many contemporary mass spectrometers. It is often paired with other ion optics to facilitate ion *m/z* isolation or used solely as a mass analyzer (e.g., triple quad and ion trap mass spectrometry). Ion isolation in a linear quadrupole is performed when the operational conditions (e.g., voltages and drive frequency) form stable environments for only a narrow range of ion *m/z*. In this respect, only the stable ions can transmit through the quadrupole. A mass filter works by dynamically changing these conditions, thus scanning through the range of stable environments wherein only stable ion *m/z*'s will transmit. The stability of an ion is determined by the Mathieu parameters *q* and *a*:

(1) $q = \frac{4ez}{mr_0^2\Omega^2}V_{AC}$ (2) $a = \frac{8ez}{mr_0^2\Omega^2}U$

where *e* is the elementary charge of a particle, *z* is the charge state of the ion, *m* is its mass, r_0 is the effective quadrupole radius, V_{AC} is the amplitude of the RF, U is the DC offset between the electrode pairs, and Ω is the radial frequency. A Mathieu space stability diagram, like the one provided in **Figure S1** is used in conjunction with the Mathieu parameters to determine if an ion is stable. In **Figure S1** an ion is completely stable only if its *q* and *a* values fall within the green shaded region which is called a stability zone.

Conventionally, quadrupole devices are driven by a resonantly tuned sinusoidal RF. In 1973, Richards remarked that the conventional sinusoidal RF driving a quadrupole device was not critical to its function and was the first to experimentally demonstrate a digital RF-driven quadrupole.[1] While promising, the limitations of the waveform modulation techniques available to Richards at the time prevented further investigations. A modern digitally operated quadrupole mass filter (DMF) was first demonstrated in 2018.[2–4] It was enabled by the advent of a new comparison-based waveform generator (WFG) developed by Hoffman et. al.[5] A true digital mass filter is driven by rectangular waveforms that are defined by a duty cycle, which is the percentage the waveform cycle is in the high state. When operated digitally, the duty cycle affects the ion stability similarly to that of the resolving DC offset.[6,7] Traditional sine-driven mass filters operate at constant frequency and navigate the stability diagram by scanning U and V_{AC} simultaneously at a fixed ratio. On the other hand, the DMF operates by manipulating the duty cycle and scans the drive frequency at a constant V_{AC}.[8] Because digital quadrupole devices navigate stability through a near-instant change of duty cycle and frequency, rather than voltages, there are operational advantages over conventional devices that make them appealing. For example, digital

quadrupoles can store and isolate large biomolecules by reducing the drive frequency at constant AC voltage as opposed to the conventional approach, which requires increasing the operational AC voltages and scanning the DC voltage to their experimental limits.[9–14] Just as quickly as the frequency can be reduced using digital RF modulation techniques, it can be increased to accommodate the lower *m/z* mass range. In other words, digital operation permits facile change of the stable mass window through an instantaneous change of drive frequency. Conventional sine-driven quadrupoles can also operate at lower frequencies to accommodate larger *m/z* ions; however, a drawback is they are not able to rapidly interchange between frequencies because physical hardware changes are required.[8,15] This property of a low *m/z* cut-off rather than a higher *m/z* cut-off is unique to digitally operated quadrupole techniques. The lower *m/z* limit for a digitally operated quadrupole will depend on the specifications of the quadrupole, stability zone, and applied voltages, among other factors. In general, operating at a lower AC voltage lowers the low *m/z* cut-off. By operating in the higher stability zones the digital mass filter can scan through mass ranges that extend lower than is possible within the first stability region. Also appealing is that digital operation permits linear ion trap boundary scans to proceed without an auxiliary excitation voltage.[16] The ability to rapidly change ion stability in a linear quadrupole device permits the DMF to rapidly access and explore the higher stability zones; a mode of operation that is much less common when operated conventionally.[2,17–22]

A key operational condition of conventional sine-driven quadrupoles operated in the primary zone is the requirement that Mathieu parameters conform to $q < 0.908$ and $|a| < 0.237$. However, less commonly, it is possible to operate sine-driven quadrupoles in other zones of stability. For example, Douglas and coworkers utilized conventional mass filters individually and in tandem to conduct elemental analysis of ions from high energy beams in some of the higher stability zones.[23–25] In their work, they reported improved resolving powers compared to the primary zone; however, the viability of this technique to improve resolving powers over a broad mass range was greatly limited (e.g., $m/z \leq \sim 50$). Operation of conventional quadrupole mass filters in the higher stability zones is exceedingly difficult to achieve due to the extensive voltage requirements (*i.e.*, thousands of V_{AC} and U voltage) oscillating at high frequencies (*e.g.*, MHz). Other drawbacks of these higher zones are the significantly reduced acceptance and highly destabilizing fringing fields that are exacerbated by the higher operational voltages and deleterious to ion transmission.[26–29]

Because the DMF navigates stability through a change of duty cycle and frequency rather than voltage, digital operation in the higher stability zones is experimentally feasible and not

necessarily mass range limited within a given zone. For example, the DMF was able to access zone B (or region IV; Dawson's convention[28,29]), where the theoretical and experimental sensitivities were better when compared to digital operation in the primary zone for the same mass window.[2,6] When the higher zones are accessed digitally, the magnitude of the fringing fields is much lower because they are operated at much lower AC voltage (e.g., 100 V_{AC}). The low operational voltage and facile access of the higher stability zones without mass range limitation permits the exploration of zones beyond those identified by Dawson.

Following the digital mass analysis in zone B, the observed improvement of sensitivity led to an ambitious pursuit to map and test stability zones beyond those previously explored or defined in the literature.[30–32] This pursuit then required an improved convention to assign and discuss the new zones.[20] The new convention, portrayed in **Figure 1**, describes the overlap between the orders of the stable regions of the *x* and *y*-axes. In the new convention, the stable regions ($a \geq 0$) described by Dawson[28,29] as I, II, III, and IV are now (1,1), (2,2), (2,1), and (3,3), respectively. In addition to the four zones identified by Dawson, **Figure 1** features two additional zones, (3,1) and (3,2), that were recently experimentally accessed for the first time as demonstrated by Chakravorty et. al.[21]

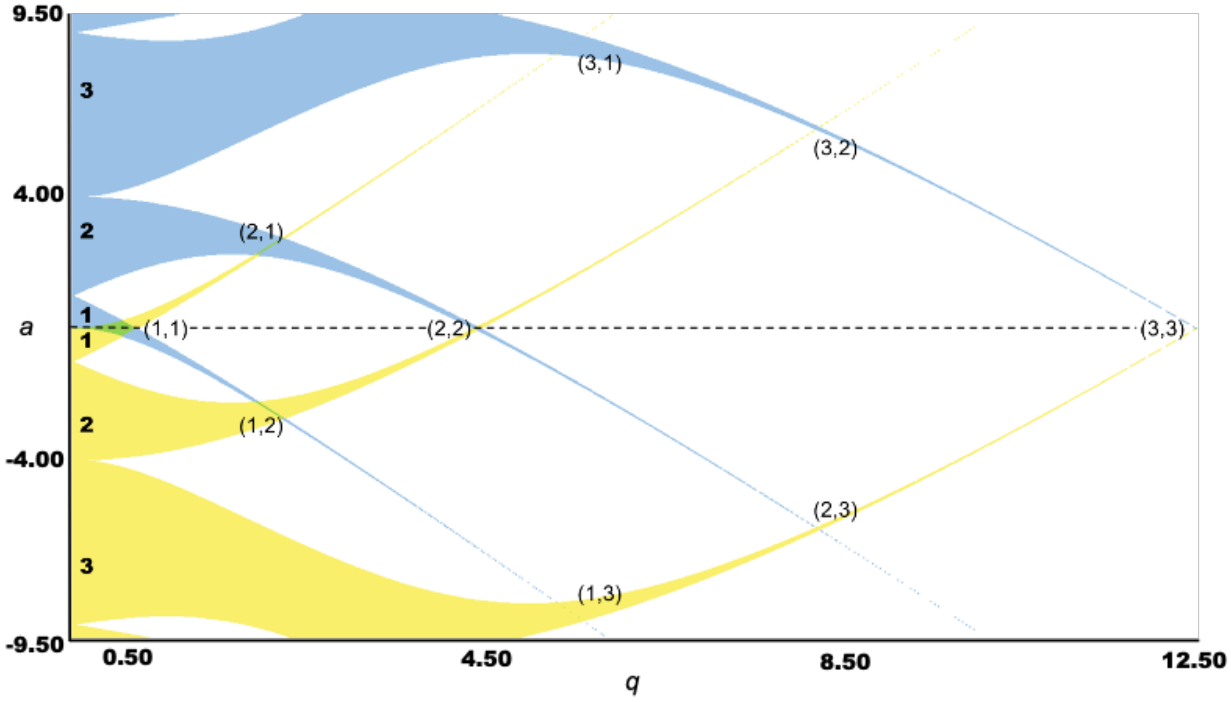

Figure 1: The Mathieu space stability diagram emphasizing some of the higher-order stability zones. This particular diagram is of a square rectangular RF waveform and is similar to that of a conventional sine-driven mass filter. When operated digitally each of the identified stable zones can be moved to the a = 0 line using a duty cycle. When a duty cycle is used, there is no need to apply a DC offset between the electrode pairs. At a = 0 the zones are accessed horizontally using a fixed AC voltage and ions are scanned by sweeping the frequency.

To create isolation windows with digital RF, a duty cycle is varied rather than the DC voltage between rod pairs. The purpose of the duty cycle is to manipulate the stability zones so that their desired isolation windows are at *a* = 0. An example of this manipulation and the newly accessed zones are featured in **Figure S2**. To access the (3,1) zone digitally, 83.33/16.67 duty cycle waveforms are used to translate the zone onto the *a* = 0 line in Mathieu space which leads to an operational *q* value of 4.5 (see **Figure S2A**). Similarly, when the duty cycle is 62.5/37.5, the (3,2) zone intersects the *a* = 0 line at a *q* value of 8 (**Figure S2C)**. In **Figures S2A** and **S2C**, ions are stable along both quadrupole axes only when their Mathieu parameter values fall within the green-shaded regions; however, when operated digitally, the accessible range of stability is defined by the span of *q* values that intersect *a* = 0. Small changes to the duty cycle can be used to change the range of stable *q* values; however, the greatest sensitivity occurs when the *q* value intersects the midpoint of the zone.[18,20] From **Figures S2A** and **S2C**, the range of stable *q* values (at *a* = 0) is small. As a consequence, when operated digitally, the mass windows of these zones are also quite small (see **Figures S2B** and **S2D**). However, because the DMF scans the

operational frequency, the windows of these zones are moved across the entire mass range of the sample. The relatively narrow mass windows of these zones make them suitable for high-resolution mass analyses.

The reproducibility and precision of the applied waveforms are the primary limitations for accessing these narrow stability zones. In other words, the jitter of the waveform must be low enough that the stable mass window does not shift stochastically during analysis.[21] Based on previous observations of the impact of waveform jitter in operating in zones (3,1) and (3,2), recent advances to hardware and the comparison-based waveform generation method were made to reduce the waveform jitter to ~10 ppm,[21] permitting reliable access to the (3,1) and (3,2) zones. Additional details of the WFG can be accessed in the Supplemental Information.

In this work, the (3,1) and (3,2) zones were accessed using higher-resolution waveforms and the outlined experiments explore and characterize the the behavior of ions in these zones using EI-generated perfluorotributylamine fragment ions. First, the improved performance of the (3,1) and (3,2) zones were compared when the higher-resolution waveforms were used. In addition, a characterization was made of the effect of several beam energies as well as the AC voltage on the attainable resolving power (RP), signal-to-noise (SN), and number of RF cycles that ions must reside in these higher zones to achieve higher degree of separation between stable and unstable ions. Using a refined WFG mechanism, this present work evaluates the temporal effects of the digital mass scan parameters on SN, peak fidelity, and scan duration for the (3,1) and (3,2) stability zones.

Experimental

Chemicals and Instrumentation

Perfluorotributylamine (PFTBA) was purchased from Scientific Instrument Services Inc. (Ringoes, NJ, USA) and used unaltered. PFTBA vapor was metered into the vacuum chamber using a leak valve connected directly to the ion source. While the absolute leak rate was not explicitly measured, this level was held constant across the experiments presented and controlled to provide reasonable signal levels and minimize carry-over. PFTBA fragment ions were generated by electron impact (EI) ionization. The PFTBA fragments were then transferred to a digitally operated SCIEX (r_0 = 4.17 mm, I = 203 mm) analyzing quadrupole (AB SCIEX, Concord, Ontario, Canada) where the ions were filtered by *m/z*. The transmitted ions were then detected by an electron multiplier (EM) conversion dynode (CD) pair. In this configuration, the EM and CD

potentials were -2,200 V and -4,000 V, respectively. The generated signal was then amplified by a Keithley 428 current amplifier (Tektronics Inc., Beaverton, OR, USA) operated with a gain of 10^6 V/A. The operating pressure of the DMF and detector was $7.5x10^{-6}$ Torr.

The comparison-based method of low-voltage digital waveform generation has been described previously.[12,21,33,34] Briefly, low-voltage digital waveforms were generated via the comparison-based method[5] by the Astraea waveform generation platform (Gordon A. Anderson Custom Electronics LLC, Kennewick, WA). The platform provided the 5 V gate input waveforms to drive a pair of DEI PVX-4150 (Directed Energy, Inc., Fort Collins, CO, USA) high-voltage switches. These switches were backed by a pair of Glassman (High Voltage Series FX 300W) power supplies (High Bridge, NJ, USA), and the resulting high-voltage digital waveforms were used to drive the DMF (e.g., 50 - 200 $V_{0\text{-}p}$). In this work, all mass spectra were acquired using Astraea's built-in acquisition feature. The frequency of these RF waveforms was swept in the scan in the range of 50 kHz to 500 kHz depending on the AC voltage and which stability zone the mass filter operates in due to the change in *q* value.

Digital Mass Scanning.

A digital mass scan is different than the scan of a conventional mass filter. When operated digitally, the AC voltage is fixed, and the duty cycle of the rectangular waveform is used to transform the Mathieu space stability zone to the $a = 0$ intersection. A duty cycle is the percentage of the waveform cycle of an axis in the high state. For example, a 60/40 duty cycle means the waveform of the first axis is high for 60 percent of the applied cycle, and the second axis which in this case is high for 40 percent of the cycle. Because the duty cycle translates the working area of Mathieu space to the $a = 0$ line, there is no need to apply a DC between the electrode pairs. To scan through a range of *m/z* values, the frequency, rather than the AC voltage, is scanned, which alters the experimentally realized *q* value. Initially, the frequency of the mass filter is set to the value needed for the ion *m/z* at the scan start to be at the deepest part of the pseudopotential well. The frequency is then stepped lower (e.g., increasing *m/z*) by an increment that is defined by the user-defined mass step size. The mass filter pauses at each frequency (or *m/z*) step for a user-determined number of waveform cycles. The scan is completed when the frequency has stepped to the value of the highest *m/z* ion of the scan. This process is portrayed generically in Figure 2 to show a 60 percent duty cycle waveform that pauses for one waveform cycle at each of five mass steps.

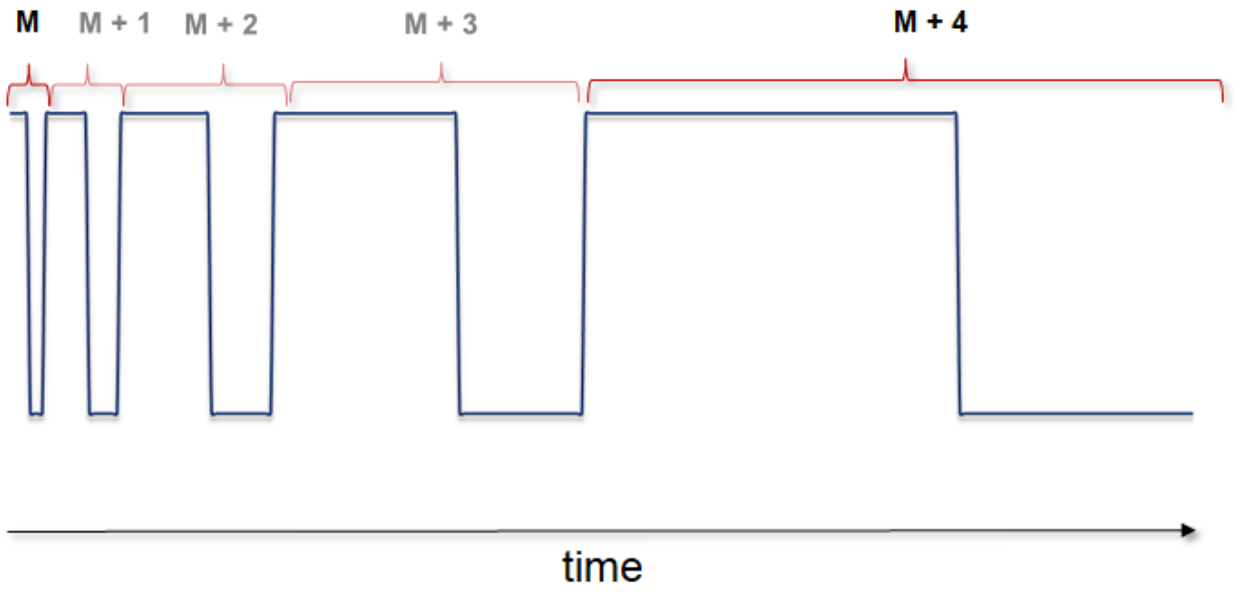

Figure 2: Simple diagram depicting a scanning digital waveform. Here, the frequency of a 60 % duty cycle waveform is scanned from high to low (increasing *m/z*) with a unit-wide mass step and a five-unit range. At each mass step, the waveform frequency is maintained for one cycle.

Data Processing

The experimental FWHM RPs cited in this work were found using the FWHM and centroid values reported by the Origin Lab software (OriginLab Corporation, Northampton, MA, USA) after peaks were fit to a Gaussian distribution.

Results and Discussion

Jitter Improvement

Historically, a limitation for the DMF to access stability zones greater than (2,1) has been the reproducibility of the waveforms. The first generation WFG reported by Hoffman et. al.[5] produced waveforms of ~100 ppm resolution. These waveforms were more than adequate to access the (1,1) and (2,1) stability zones. However, because the method relied upon the comparison against direct digital synthesis (DDS) generated sine waves the resolution was not constant throughout the range of frequencies and duty cycles. To maintain a constant ~100 ppm resolution over the full range of frequencies and duty cycles, improvements were made to the waveform generation

method by comparing against DDS-generated triangular waveforms.[5] Previous efforts evaluated waveform jitter on the stable mass windows of the (3,1) and (3,2) zones, concluding better waveform resolution was required.[21] Building upon these results, the WFG was re-engineered by GAA Custom Electronics, LLC to produce more precise waveforms (e.g., ≤ 10 ppm) over the range of operational frequencies. These waveforms now permit sensitive experimental characterization of the (3,1) and (3,2) zones. In this section, the goal is to briefly contrast the improved sensitivity enabled by the higher-resolution waveforms and then provide an initial glimpse of the (3,1) and (3,2) zones.

The improved performance of the (3,1) and (3,2) zones that was enabled by the higher resolution waveforms is demonstrated in Figure 3 which contrasts the spectral quality of the 131 *m/z* PFTBA fragment ion after it was acquired using the ~100 ppm (**Figures 3A** and **3B**) and ≤ 10 ppm (**Figures 3C** and **3D**) resolution waveforms. Although access to these zones was attainable using the ~100 ppm resolution waveforms the sensitivity was markedly degraded compared to the 10 ppm waveform. In contrast, when the spectra were acquired using the higher resolution waveforms (**Figures 3C** and **3D**) the improvement was apparent.

An additional demonstration of the performance of the higher-resolution waveforms is featured in **Figures S3A** (zone 3,1) and **S3B** (zone 3,2) which are normalized mass spectra acquired over the range of observable PFTBA fragments. Notably, the relative abundances of these fragments differ between spectra due to variations in the ion source as the represented spectra were collected days apart. Similar to **Figures 3C** and **3D**, the transmission (*i.e.*, the SN ratio of the peaks under comparable operating conditions) in the (3,2) zone is lower than in (3,1) across the spectrum which was ascertained based on the signal-to-noise of the individual peaks when compared between spectra. Although waveform reproducibility is crucial to access the full potential of these higher zones other constraints, such as the narrow acceptance apertures of the high stability zones that are worsened by the fringing fields, and the high rate of radial excitation (factors that will be discussed shortly) presently limit the attainable resolution and sensitivity.[19,26,28,29,35,36] The remainder of the present work details the impact of these constraints on performance and how factors such as the beam energy, AC voltage, number of waveform cycles, and mass step size comprising a scan affect the experimental sensitivity and resolution of the (3,1) and (3,2) zones. The 219 *m/z* fragment (see **Figures S3A** and **S3B**) of PFTBA serves

as a representative test case for the initial evaluation of higher stability zones due to its pronounced SN across zones (3,1) and (3,2).

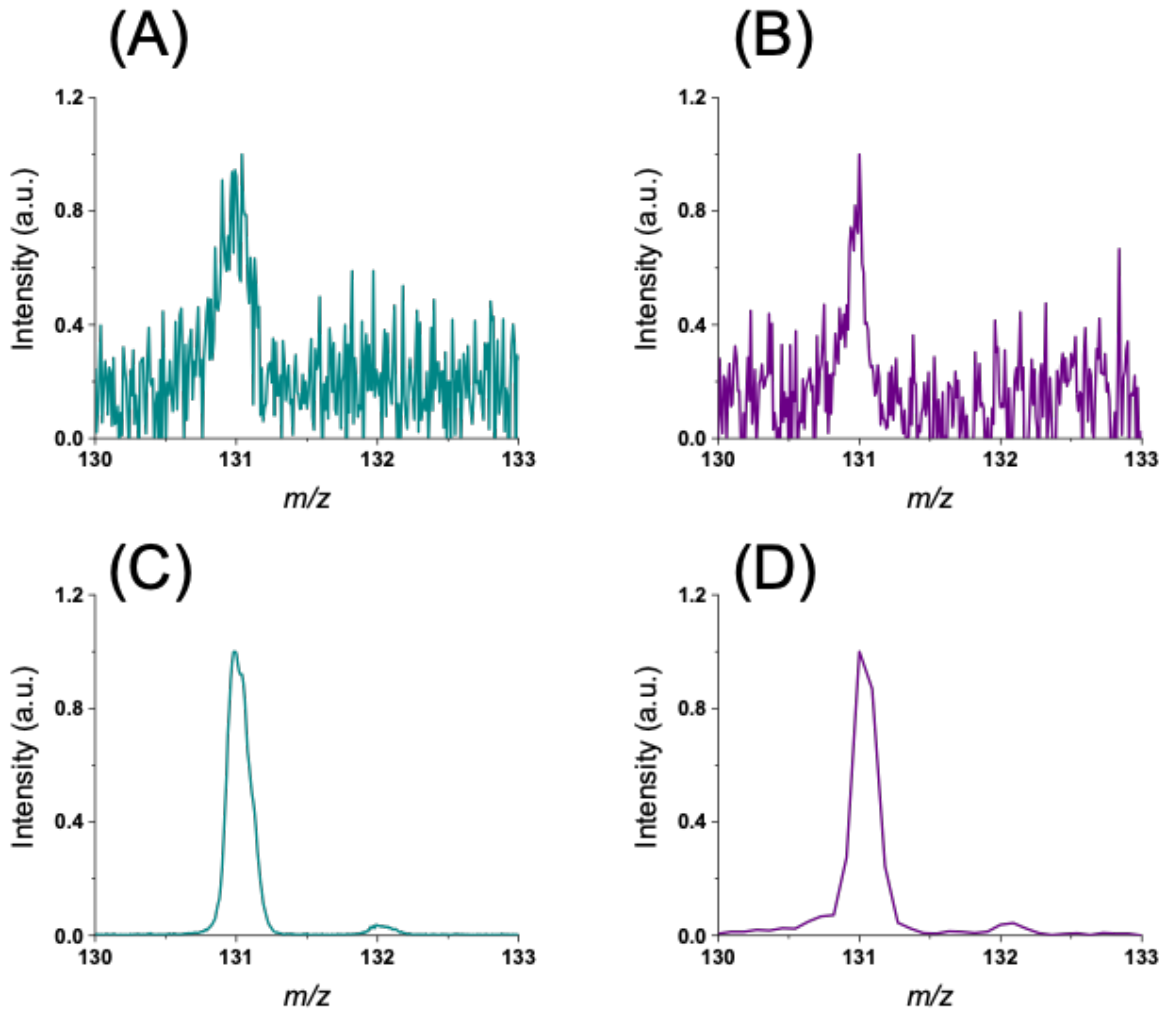

Figure 3: Comparisons the 131 *m/z* PFTBA fragment ion when it was used to experimentally access (A) the (3,1) and (B) (3,2) zones when the waveform resolution was ~100 ppm and (C) the (3,1) and (D) (3,2) zones when the waveform resolution was ≤ 10 ppm.

Resolving Power and Sensitivity

(1) *The Effect of the Beam Energy*

In each stability zone, the value of the theoretically predicted resolving power and sensitivity are generally greater than can be achieved experimentally. Theoretical values are calculated using the Mathieu parameter *q* and pseudopotential well depth.[6,7] Predicted values do not consider effects imposed by numerous experimental constraints or factors such as the quadrupole acceptance, fringing fields, and the rate of radial excitation. Acceptance defines the range of transverse trajectories stable ions can have when they enter the quadrupole. Fringing fields alter initial ion trajectories by increasing their transverse component, causing more ion trajectories to fall outside the acceptance aperture. Ions with trajectories outside the acceptance aperture are not transmitted. Slower moving ions are more affected by these fields because of their longer residence times.[37] Higher energy beams are more radially focused (e.g., fewer transverse trajectories) which helps increase the transmission of ions into the quadrupole because more ions are initially within the acceptance aperture. At higher energies ions also spend less time in the fringing regions which also improves transmission. Although transmission can be improved with increased beam energy, it can negatively affect resolution because the faster-moving ions will experience fewer RF cycles of the quadrupolar field. However, in the higher zones, the rate of radial excitation (e.g., how quickly unstable ions are radially ejected) from these fields is much greater than in the primary zone.[23,25,29,38] Due to the higher rate of radial excitation, greater beam energies can be used to inject ions into the mass filter to help overcome the destabilizing effects of the fringing fields. Although this high rate of excitation permits ion isolation in fewer RF cycles, if the beam energy is too high the ions at the bounds of stability can transmit before they are destabilized by the fields which will reduce the resolution. Therefore, it is desirable to characterize the effect of the beam energy to find a range of suitable values where increasing sensitivity has minimal impact on RP.

In the following experiment, the beam energy was varied (from 20 to 300 eV) by a similar method as described in Opačić et. al.[3] In that method, a trapping quadrupole field was used to control the energy of the ions injected into the mass filter. In this work, varying the DC axis potential of the mass filter varies the energy of the ions arriving from the ion source. Varied energy EI-generated PFTBA ions were monitored to observe the effect on the RP and SN. The results of this experiment are summarized in **Figure 4**. The RP was greatest when the beam energy was low and declined approximately linearly as it was increased (see **Figures 4A** and **4B**). The highest

RPs were obtained with a 20 eV beam and were roughly 795 and 1,942 for the (3,1) and (3,2) zones, respectively. For context, the theoretical RPs for these zones are 1,140 and 3,447 for the (3,1) and (3,2) zones, respectively. As discussed earlier, theoretical values are generally greater than those that can be achieved experimentally. At low beam energy ions spend more time in the DMF and are excited by more cycles of the RF to improve the RP. The RP obtained from these experiments declined as the beam energy was increased because ions at the edge of the stability boundary did not radially excite enough for them to radially eject before they could transmit. Consequently, as the energy was increased the ions spent fewer RF cycles in the quadrupole and the SN increased as demonstrated in **Figures 4C** and **4D**. However, unlike the predictable decrease of the RP with increasing beam energy, in this experiment, the SN increased only up to ~125 eV. The reason for this unanticipated decrease can be gleaned from the spectra collected at each of the beam energies presented in **Figure S4**. The peaks in **Figure S4** were generally uniform in their appearance when the beam energy was 125 eV or less. Above this threshold, the peaks broadened and exhibited low mass fronting. Effectively, at a given frequency and beam energy, lower mass ions do always excite to the degree to be radially ejected. Stated differently, because lower *m/z* ions have increased velocities, the number of waveform cycles these populations experience is diminished. In this particular case, the broadening eventually caused the intensities to decrease and the peak widths to exceed the acquisition window. Although the SN decreased above 125 eV the ion transmission (e.g., peak area, **Figures S5A** and **S5B**) generally continued to increase to a beam energy of about 175 eV in the (3,1) zone and 125 eV in the (3,2) zone where the peaks were no longer confined to the acquisition window. However, there was a disparity in this trend above 200 eV in the (3,2) zone.

As noted previously, the beam energy affects the ions' residence times and the number of RF cycles they excite in the field. The rate and magnitude of radial excitation, which differs in each stability zone, impact the number of RF cycles needed for optimal separation. In the higher stability zones, the rate of radial excitation is much greater compared to zone (1,1) thus allowing ion isolation in fewer cycles. To determine the optimal beam energy, the products of the RP and SN were plotted and presented in **Figures S6A** and **S6B**. From these plots, a beam energy between 75 eV and 125 eV provided isolation with an optimal balance of the attainable RP and SN. In this range ions in the (3,1) and (3,2) zones spent about 6 and 4 RF cycles in the quadrupole fields, respectively, whereas in a conventional sine-driven mass filter operated in the (1,1) zone the ions were said to experience about 60 cycles[25].

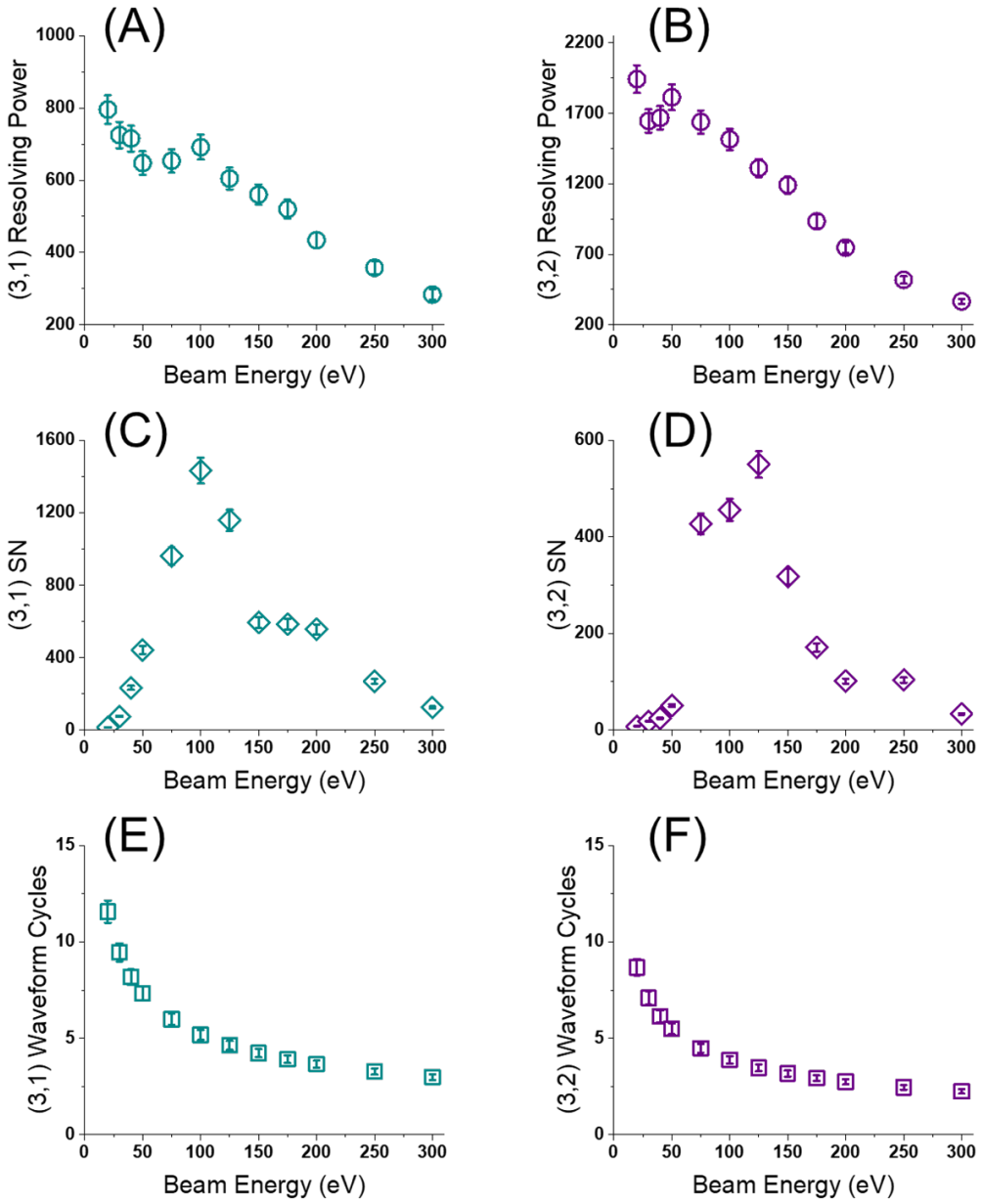

Figure 4: Plots of the measured resolving power (RP), signal-to-noise (SN) and number of waveform cycles ions spend traversing the quadrupole at several ion beam energies in the 20 – 300 eV range. The RP dependence on the beam energy of (A) the (3,1) zone and (B) the (3,2) zone. The SN dependence on the beam energy of (C) the (3,1) zone and (D) the (3,2) zone. The number of waveform cycles that ions take to traverse the quadrupole at several beam energies for (E) the (3,1) zone and (F) the (3,2) zone

.

(2) ***The Effect of the AC Voltage***

The previous section explored the effect of beam energy on the RP and SN. The experiments were all performed at 100 V_{AC}. However, the AC voltage also affects resolution and sensitivity. Increasing the AC voltage causes the pseudopotential well to deepen which according to Huntley and Reilly[6,18] will improve sensitivity, but it will also cause the magnitude of the fringing fields to increase and will require higher beam energies for ions to overcome them. When the AC voltage is increased the operational frequency must also increase for the ion *q* value to remain at the deepest part of the well. If the beam energy were held constant, the higher operational frequency would also increase the number of RF cycles ions experience in the fringing region and mass filter fields which will affect sensitivity and resolution; therefore, the optimal beam energy is dependent on the AC voltage.

Characterization of the effects of AC voltage at different beam energies was made to monitor how the RP was affected. Normalized mass spectra from this experiment are presented overlaid in **Figure S7**. The trend of the RP for the different beam energies and AC voltages are provided in **Figure 5**. When the AC voltage was 50 V the RP was greatly affected by the beam energy in both zones. As the AC voltage was increased, the RP was less affected by the beam energy. For example, when the AC voltage of the (3,1) zone was 50 V the RP varies between 161 and 551 when beam energy was varied. The range of the RP was narrower at an AC voltage of 200 V, only varying between 706 to 754 when adjusting the beam energy. While the RP was most consistent throughout the range of beam energies when the AC voltage was 200 V; the sensitivities were disparate, as can be observed by the variation of the noise in **Figure S7C**. A similar progression was observed for the (3,2) zone; however, during an initial assessment, transmission was lost when the AC voltage was 200 V. This loss was likely due to the increased destabilizing effects of the (3,2) zone fringing fields caused by the increased AC voltage. Therefore, to adequately capture the trend in the (3,2) zone different AC voltage and beam energy combinations were used. In the (3,2) zone there is more variation of the RP at each of the AC voltages. For example, when the DMF was operated at 50 V_{AC} the RP decreases with increasing beam energy, noticeably. Over the range of three beam energies, RP at 50 V_{AC} ranges between 230 and 1134 unlike at an AC voltage of 100 V where the RP is much more consistent over the range of beam energies. At 100 V_{AC}, the RP varies between 1172 and 1371 over the three beam energies. In general, the variation of the RP over the span of beam energies from both zones decreased as the AC voltage was increased; however, as noted, the variation from the (3,2) zone was persistently greater throughout the range of AC voltages. The variation of the RP from the

(3,2) zone is likely the consequence of the low jitter that persists in the waveforms combined with the narrow overlap of the *x* and *y* stability wells.[21] Jitter causes the wells to shift slightly and the range of stable masses to oscillate at the picosecond scale. This oscillation affects the RP because it leads to a slight variation in the range of masses that are transmitted at any given time. In the (3,2) zone, the RP was more consistent over the range of beam energies as the AC voltage was increased. This is largely attributed to the concept that stable ions near the boundaries of these oscillating wells became transiently unstable during the oscillations. In this context, a transiently unstable ion is defined as an ion that is momentarily moved outside the stable boundary by the waveform jitter. Unstable ions fall outside the stable boundary and should not transmit; however, because these ions are unstable momentarily, the magnitude of excitation, which is affected by the AC voltage, will affect how quickly an ion radially excites. The time the ions spend in the quadrupole and the magnitude of excitation determine whether the ions radially eject or re-stabilize. At lower AC voltage (e.g., 50 $V_{0\text{-}p}$), the RP was less consistent because more weakly stable ions were able to completely pass through the mass filter while they were transiently unstable. Because the reduced AC voltage also reduces the excitation magnitude, weakly stable ions are more likely to completely pass through the mass filter while they are transiently unstable. In this sense, at lower AC voltage the waveform jitter creates a virtual widening of the stable well overlap. Conversely, because weakly stable ions can be lost during the well oscillations, the jitter at higher AC voltage creates a virtual narrowing of the stable well overlap. Because the jitter is inherently random with each RF cycle the number of metastable ions that can be lost or transmitted is also random with each RF cycle, leading to these variations.

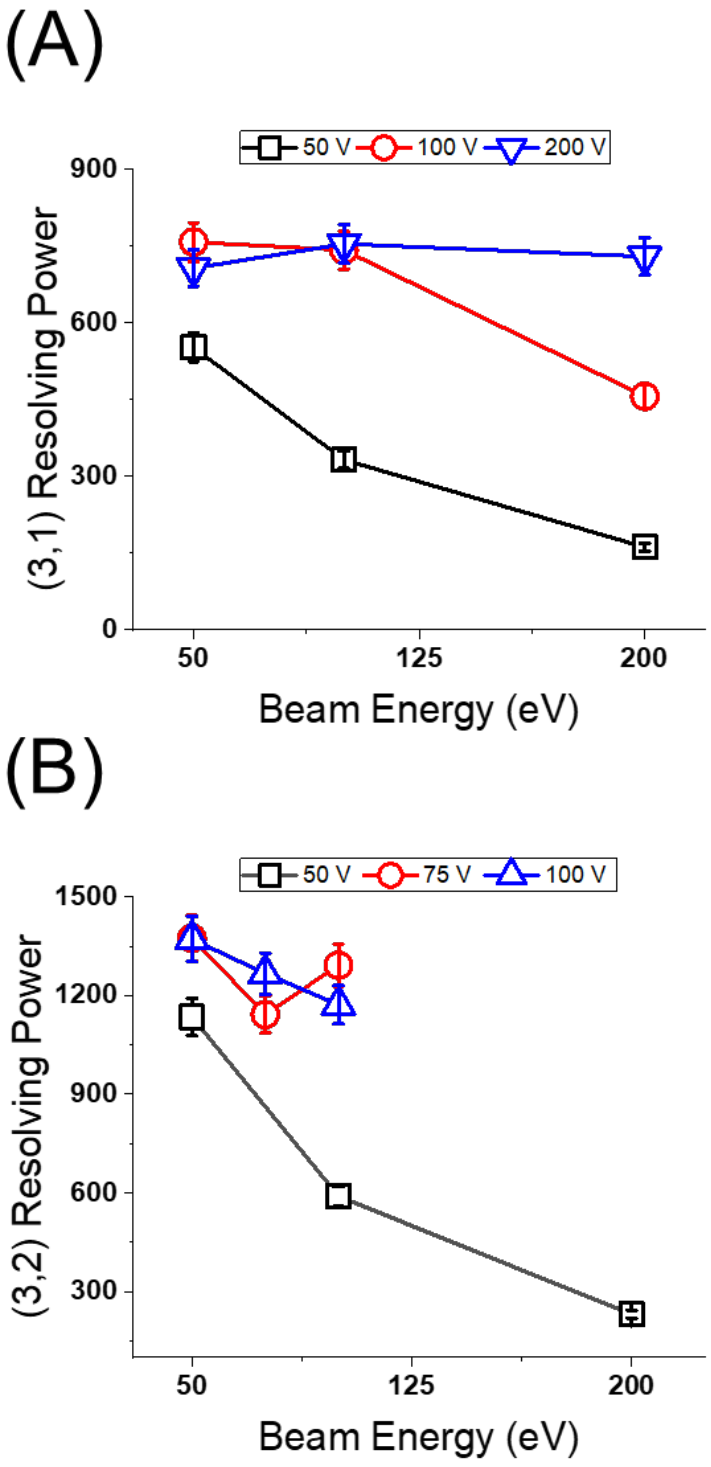

Figure 5: The effect of beam energy on the RP at different AC voltages for (A) the (3,1) zone when the AC voltage was 50 V (black), 100 V (red) and 200 V (blue) and (B) the (3,2) zone when the AC voltage was 50 V (black), 75 V (red) and 100 V (blue).

(3) ***The Effect of Waveform Dwell and Width of a Mass Step***

Beam energy affects the residence times of ions and, consequently, the number of RF cycles they will experience in the quadrupolar fields of the higher stability zones. To achieve the best possible resolution, ions at the bounds of stability must excite and radially eject before they can traverse the length of the DMF. The rate of unstable ion excitation will affect the range of beam energies that provide a balanced separation. This range of beam energies depends on the AC voltage because the waveform frequency must change to accommodate the *q* value at the deepest part of the pseudopotential well. When operated digitally, ions are isolated by scanning the waveform frequency while keeping the amplitude of the AC voltage constant. A DMF scans a mass range from low to high *m/z* by stepping the frequency of the AC voltage from high to low by a user-defined value. If the frequency of the DMF is conducive for an ion to have a stable *q* value, the ion will transmit. Although the frequency of the AC voltage decreases during a scan, when the beam energy is constant, each ion spends the same number of waveform cycles in the DMF because the velocity of the stable *m/z* ions decreases with frequency. In this respect, the number of waveforms comprising a step of a scan (waveform dwell) sets the limit on the number of ions that can be transmitted in a step. Because each step of the scan is defined by the same fixed number of waveforms, each ion is uniformly sampled, and the relative abundance of each ion in the sample is preserved. When the DMF scans a continuous ion beam, the waveform dwell can be used to compensate for samples having either low or high abundances by increasing or decreasing the waveform dwell. Presently, the WFG cannot dynamically change the waveform dwell during a scan so it is not able to selectively increase the abundance of an ion population derived from a continuous ion beam. The DMF can be used to scan the entire spectrum of a sample or to isolate a specific range or individual ion *m/z*. The scanning mode and its parameters affect the quality, sensitivity, and duration of an acquisition. In the following experiments, the effects of the waveform dwell, and mass step size on the SN and scan duration were explored.

Mass spectra of PFTBA fragment ions from the (3,1) and (3,2) zones were acquired using a 0.09 *m/z* step over a range of waveform dwell values (50 – 2500 waveforms per mass step). As the waveform dwell was increased, more ions were sampled at each mass step, leading the SN to increase. The impact of increasing the waveform dwell on the SN can be dramatic. For example, when the waveform dwell was increased from 50 to 2500 the SN of the 219 *m/z* ion sampled from the (3,1) zone improved by a factor of about 18. The SN factor increase of the 219 *m/z* ion for several waveform dwell values between 50 and 2500 are presented in **Figures 6A** and **6B** for the (3,1) and (3,2) zones, respectively. The SN factor increase was found by dividing

the SN measured from each dwell value by the SN measured from the lowest dwell value. In both stability zones the SN continued to increase with the value of the waveform dwell; however, the change in the factor increase of the SN lessened between each increase of the waveform dwell. Increasing the waveform dwell improved the SN, but it also extended the duration of the scans. When the waveform dwell is used to enhance the sensitivity of spectra acquired from a continuous source, it is most efficient to operate in the range where the SN increase is linear with each increase of the waveform dwell to avoid unnecessarily prolonging the scan. In the (3,1) and (3,2) zones there is an observable linear improvement up to a waveform dwell of 500 and 250, respectively. For reference, mass spectra acquired when the waveform dwell was 50 and at the upper bound of the linear improvement range are provided in **Figures S8** and **S9** for the (3,1) and (3,2) zones, respectively. As noted, the duration of a mass scan is primarily affected by the waveform dwell and the number of mass steps which will vary by the sample, stability zone, and objectives of the experiment. In this work, a scan that consisted of 0.09 *m/z* steps spanning the 60 – 600 *m/z* range and used a waveform dwell of 250 corresponded to scan durations of 7.37 and 9.87 seconds for the (3,1) and (3,2) zones, respectively. Similarly, when the waveform dwell was 50, the scan proceeded in 1.48 and 1.98 seconds for the (3,1) and (3,2) zones, respectively. Although the waveform dwells were the same for each zone in these comparisons the (3,2) scan durations were longer because the operational frequency was lower compared to the (3,1) zone.

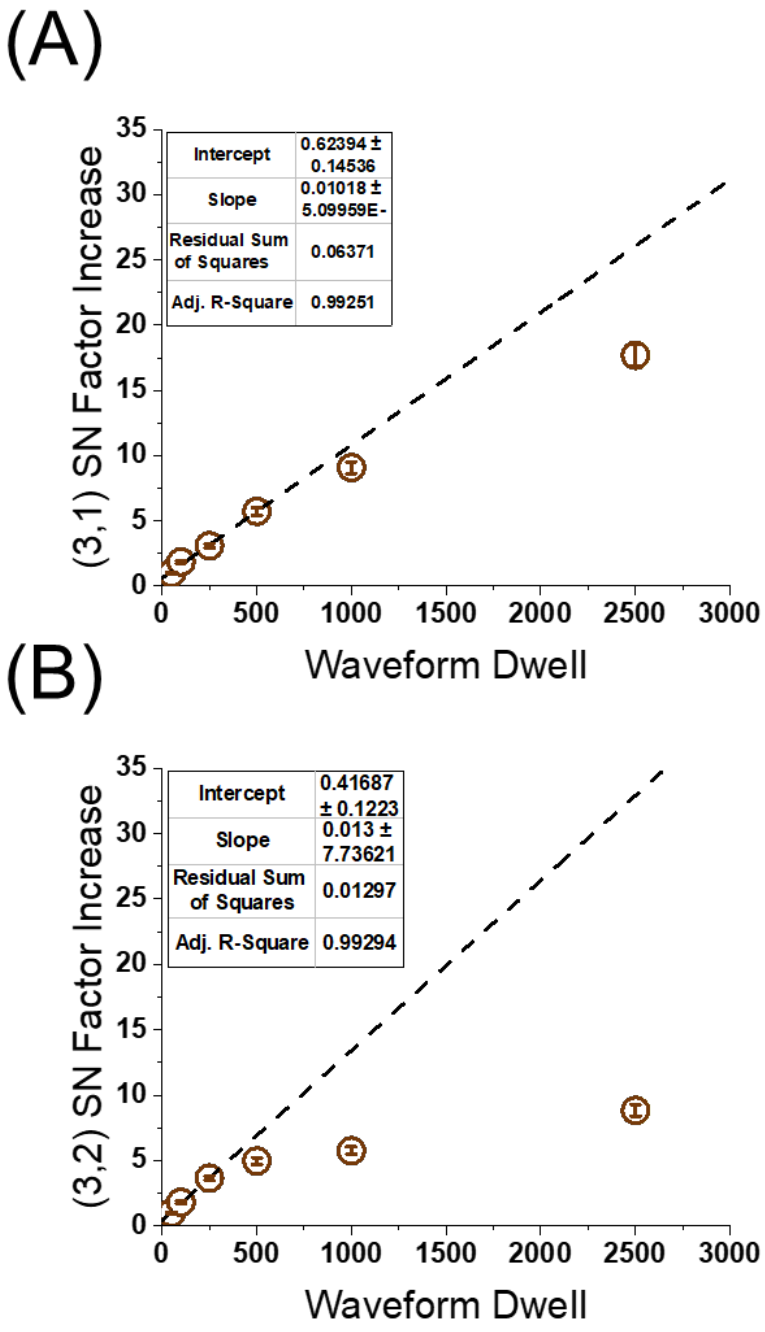

Figure 6: The SN factor increase as the waveform dwell was increased for (A) the (3,1) zone and (B) the (3,2) zone. The SN factor increase was found by dividing the SN from each dwell value by the SN when the dwell was 50. The linear range of improvement extends to a dwell of 500 for the (3,1).

Operation of the DMF with excessive waveform dwell greatly affected the duration of the mass scans but also negatively impacted the SN. For example, in the (3,2) zone, the factor increase of the SN began to plateau when the waveform dwell was greater than 250. Ideally, each increase of the waveform dwell should continue to improve the SN because more ions are transmitted; however, when the waveform dwell was used alone (e.g., without averaging), more noise was introduced at each mass step, reducing the effectiveness of the technique. Averaging multiple scans acquired at a dwell value within the linear range further improves the SN. However, when replicates were averaged using small dwell values (<50) there was no observable improvement to the SN.

Similar to improving the SN by increasing the waveform dwell, the fidelity of the mass scan (e.g., how well peaks are defined) can be enhanced by decreasing the width of the mass step. In general, the mass scan is set up to sample a number of points to form a peak, however, the number of points and the peak shape itself can be subjective. When the step size is reduced, the overall number of steps comprising the scan is increased; therefore, the duration of the scan is extended. Depending on the characteristics of the sample and the zone of operation, it may be necessary to adjust the step size to increase the peak fidelity. If a peak is too narrow for a chosen mass step, it will be under-sampled and less accurately defined. Conversely, if the step size is too small, the scanned mass range is oversampled, and more noise may be acquired. Generally, as the order of the stability zone is increased, the theoretical and experimental RPs increase, so the size of the mass step should be reduced. For example, when mass analysis proceeds from the (3,1) zone to the (3,2) zone, the step size should be decreased because the theoretical RP increases from 1,140 to 3,447 in the transition.

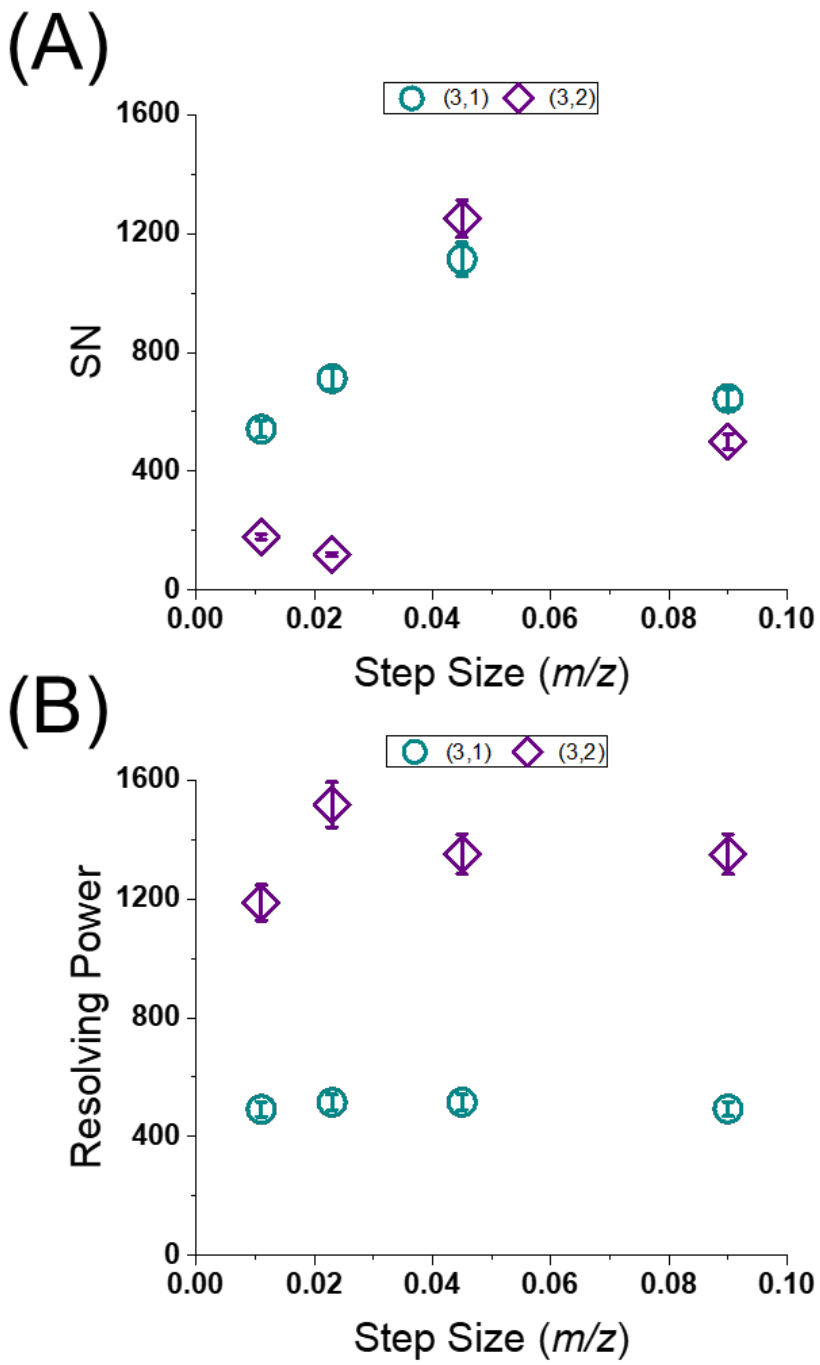

Figure 7: (A) The SN of the 219 *m/z* PFTBA ion from the (3,1) (teal) and (3,2) (purple) zones at different *m/z* step sizes. (B) The RP of the 219 *m/z* PFTBA ion from the (3,1) (teal) and (3,2) (purple) zones at different *m/z* step sizes.

To characterize the effect of the step size, the scan was set to measure the 60 – 600 *m/z* range of the PFTBA fragment ions in the (3,1) and (3,2) zones using four step sizes (0.09 *m/z*, 0.045 *m/z*, 0.023 *m/z,* and 0.011 *m/z*) and monitored the RP and SN of the 219 *m/z* ion. The spectra from this experiment are provided in **Figures S10** and **S11** for the (3,1) and (3,2) zones, respectively. The most notable observation was the gain in the SN of the 219 *m/z* ion when the step was decreased from 0.09 *m/z* to 0.045 *m/z,* followed by its decline when the step was reduced further (see **Figure 7A**). When the step size was reduced, there was a proportional increase in the number of acquisition steps which initially caused the SN to increase as well as the peak fidelity to improve. However, when the step size was less than 0.045 *m/z* the peak became over sampled and the SN declined because a greater amount of noise was acquired. In the (3,2) zone these effects are more noticeable. Here, the trend was the same; the SN increased to a step size of 0.045 *m/z* because the peak was better defined but then declined when the step size was further reduced because the noise in the spectrum was oversampled.

The theoretical RP is much greater in the (3,2) zone, potentially causing the effect of an inadequate step size to be more prominent. **Figure 7B** shows the RPs obtained in the (3,1) and (3,2) zones over the span of step sizes. In the (3,1) zone the RP was for the most part constant over the range of step sizes, having an average value of 504 and an RSD of 0.0266. In the (3,2) zone more variation in the RP was observed at the smaller step sizes, yielding an average value of 1,351 and an RSD of 0.0997. In the (3,2) zone the smaller step size caused variation in the measured RP because the jitter, although low, caused the stable mass wells to fluctuate slightly.

As noted, the step size affects the number of mass steps comprising a scan which will increase its duration. Unlike increasing the waveform dwell, the duration of the mass scan increases linearly with the number of mass steps. Therefore, the scan duration will scale with the number of mass steps.

Conclusions

Using a re-engineered, sub-10-ppm digital waveform generator, this report details the impact of the AC voltage, beam energy, and waveform dwell on several metrics of a digital quadrupole mass filter operated in zones (3,1) and (3,2). Minimizing waveform jitter reduced the sporadic shifts of the stability wells observed in prior efforts, which resulted in increased metastable overlap and improved ion transmission. Most importantly, without improvement of waveform jitter, zones (3,1) and (3,2) could not be accessed. While the scanning rates of the current digital waveform driver do not exceed those of the sinusoidal counterpart, it is important

to recognize that using digital waveform technology (DWT) within a system does not preclude sinusoidal operation. Moreover, given the broad functionality of quadrupole-based systems, the pursuit of DWT for high-resolution isolation and rapid *m/z* window transitions using higher stability zones requires continued evaluation of these instrumental modes of operation.

The higher stability zones are notorious for their narrow acceptance apertures, highly defocusing fringing fields, and high rate of radial excitation that overall lead to reduced transmission. When operated digitally, the strength of the fringing fields from these zones is minimized because the AC voltage is constant and much lower (e.g., < 200 V) than the conventional sine-driven quadrupole. However, due to the high rate of radial excitation in these zones, the fringing fields can still inhibit the transmission of ions. On the other hand, the higher rate of radial excitation causes the unstable ions to radially eject in fewer RF cycles; therefore, higher energy beams can be used to overcome the deleterious effects of the strongly defocusing fringing fields. The utility of injecting ions into the DMF over a range of beam energies was evaluated and, in each zone, the experimental RP was greatest when the beam energy was 20 eV; however, the SN was low enough that operating at 20 eV was deemed not analytically useful. When the AC voltage was 100 V there was a balance of the attained RP and SN when the beam energy was within a 75 – 125 eV range. For example, when the beam energy was 100 eV the measured RP and SN were 690 and 1,430, respectively for the (3,1) zone and 1,510 and 460, respectively for the (3,2) zone. Higher beam energies improve transmission in two ways: first, they help to radially focus ions so that more are initially within the acceptance aperture and second, they reduce the ions' residence times in the destabilizing fringing fields. The beam energy also affects the number of RF cycles ions spend in the DMF which affects the RP and SN. For example, when a 100 eV beam was used to inject ions through a 100 V_{AC} DMF they spent 6 and 4 RF cycles in the (3,1) and (3,2) zones, respectively. That beam energy and consequently, the number of RF cycles provided separation that was balanced.

Increasing the AC voltage increases the pseudopotential well depth, which improves transmission. Conversely, higher AC voltage increases the magnitude of the fringing fields that can cause ions to destabilize and have trajectories outside the acceptance aperture, which reduces transmission. The effect of the AC voltage over a range of beam energies was evaluated to measure sensitivity and RP. In both zones, the average RP increased with AC voltage regardless of the beam energy; however, the ion intensities from the lower energy beams decreased when the AC voltage was increased. In both zones, the RP varied with beam energy. This variation was more pronounced in the (3,2) zone and was likely caused by the low jitter that

persists in the waveforms, causing the overlap of the stable wells to oscillate slightly. This oscillation caused slight disparities in the range of stable masses, leading to a virtual narrowing (higher AC voltage) or widening (lower AC voltage) of the stable well overlap, causing the RP variations.

The DMF can be used to scan the entire spectrum of a sample or isolate a specific range or individual ion *m/z*. The scanning mode and parameters affect the quality, sensitivity, and duration of an acquisition. The characterization of the higher zone DMF presented in this work was completed with an overview of the effects of the scan parameters. The DMF scans by stepping the waveform frequency lower by an amount defined by the size of the mass step. At each step, stable ions transmit for a defined number of waveform cycles (waveform dwell) before stepping lower to the next frequency. The SN over a broad range of waveform dwell values was evaluated, and what was determined was that SN increased linearly with the waveform dwell when the values were less than 500 and 250 for the (3,1) and (3,2) zones, respectively. Increasing the waveform dwell beyond the linear range of improvement caused noise present during the acquisition to be oversampled, reducing the SN improvement. The waveform dwell affects the scan duration. When the waveform dwell was 250 the duration was 7.37 and 9.87 seconds for the (3,1) and (3,2) zones, respectively.

The theoretical and experimental RPs increase with the order of the stability zone. To adequately capture an ion peak, the size of the mass step must be reasonable to maintain peak fidelity and without compromising SN. By evaluation of the effect of four mass step sizes (0.09 *m/z*, 0.045 *m/z*, 0.023 *m/z,* and 0.011 *m/z*), it was determined that the SN increased initially as the step size was decreased from 0.09 to 0.045 *m/z* but then declined as the step was further reduced. The decline of the SN was likely due to oversampling of noise present during the acquisition and was worse from the (3,2) zone. The RPs from each zone were less affected by the step size. In the (3,1) zone, the RP was constant over the range of step sizes; however, there was more variation of the RP from the (3,2) zone.

A limiting factor of this work was the strong fringing fields and narrow acceptance apertures of the higher stability zones that negatively impacted ion transmission and the attainable RP and SN. Higher than normal beam energies (e.g. > 4 eV) were used to focus ions and overcome the strong defocusing effects of the fringing fields. Unfortunately, higher beam energies minimize the attainable RP due to reduced residence times of ions as they pass through the mass filter. Future work will be aimed at minimizing the impact of defocusing effects so that the beam energy can be lowered to realize the attainable RP without comprising SN.

In addition, now that these higher stability zones are readily attainable using digital waveforms, the performance of the digitally operated mass filter in isolating large molecules near and past the limit of the conventional sinusoidal mass filter can be studied. This follows the idea that the performance shown in the low *m/z* region should translate to the higher *m/z* region without loss in performance. However, higher *m/z* ions are often multiply charged which may introduce larger degrees of coulomb repulsion of the beam which can cause the envelope to widen spatially (e.g., reduce sensitivity because more ions are outside the acceptance). Higher beam energy may overcome this widening to an extent. However, it is possible that, at high charge densities, the level of improvement may be insufficient to prevent ions from exceeding the spatial constraints of the acceptance. In short, higher charge state ions may reveal a quasi-charge capacity limitation in these higher zones. Nevertheless, the lower operating voltages and capacity to access higher *m/z* values warrant the continued investigation of digital waveform technologies for mass spectrometry.

In Memoriam

The late Dr. Peter T.A. Reilly is the inspiration behind this effort. His dedication and perseverance were instrumental in the development of digital waveform-driven quadrupole technologies and techniques. Respected and admired in the field of mass spectrometry and technology development, Peter T.A. Reilly is cherished as a dear friend, mentor, and colleague. His passion for digital mass spectrometry lives on through numerous friends, students, colleagues, and the continued advancement of the technique.

Associated Content

Supporting information that contains additional figures of stability zones, plots of mass spectra from the (3,1) and (3,2) zones, peak areas, and the RP * SN dependence on beam energy. Additional technical details for the WFG provided by GAA Custom Electronics, LLC are provided as Supplemental Information.

Acknowledgments

The authors would like to acknowledge support from the National Science Foundation award #2103645, Phase I funding from the Washington Research Foundation, and both technical and material support from SCIEX.

References

(1) Richards, J. A.; Huey, R. M.; Hiller, J. A New Operating Mode for the Quadrupole Mass Filter. *International Journal of Mass Spectrometry and Ion Physics* **1973**, *12*, 317–339.

(2) Opačić, B.; Huntley, A. P.; Clowers, B. H.; Reilly, P. T. A. Digital Mass Filter Analysis in Stability Zones A and B. *Journal of Mass Spectrometry* **2018**, *53*, 1155-1168. https://doi.org/10.1002/jms.4295.

(3) Opačić, B.; Hoffman, N. M.; Clowers, B. H.; Reilly, P. T. A. Impact of Injection Potential on Measured Ion Response for Digitally Driven Mass Filters. *International Journal of Mass Spectrometry* **2018**, *434*, 1–6. https://doi.org/10.1016/j.ijms.2018.08.009.

(4) Opačić, B.; Hoffman, N. M.; Gotlib, Z. P.; Clowers, B. H.; Reilly, P. T. A. Using Digital Waveforms to Mitigate Solvent Clustering During Mass Filter Analysis of Proteins. *J. Am. Soc. Mass Spectrom.* **2018**, *29* (10), 2081–2085. https://doi.org/10.1007/s13361-018-2012-0.

(5) Hoffman, N. M.; Gotlib, Z. P.; Opacic, B.; Clowers, B. H.; Reilly, P. T. A. A Comparison Based Digital Waveform Generator for High Resolution Duty Cycle. *Rev Sci Instrum* **2018**, *89* (8), 084101. https://doi.org/10.1063/1.5004798.

(6) Huntley, A. P.; Reilly, P. T. A. New Tools for Theoretical Comparison of Rectangular and Sine Wave Operation of Ion Traps, Guides and Mass Filters. *J Mass Spectrom* **2020**, *55* (12), e4661. https://doi.org/10.1002/jms.4661.

(7) Huntley, A. P.; Reilly, P. T. A. Quantifying the Operation of Sinusoidal Mass Filters. *J Mass Spectrom* **2021**, *56* (2), e4703. https://doi.org/10.1002/jms.4703.

(8) Hoffman, N. M.; Gotlib, Z. P.; Opacic, B.; Huntley, A. P.; Moon, A. M.; Donahoe, K. E. G.; Brabeck, G. F.; Reilly, P. T. A. Digital Waveform Technology and the Next Generation of Mass Spectrometers. *J Am Soc Mass Spectrom* **2018**, *29* (2), 331–341. https://doi.org/10.1007/s13361-017-1807-8.

(9) Reilly, P. T. A.; Chen, H.; Wang, X.; Donahoe, K. G. E. High Resolution TOF-MS of Intact Singly Charged Proteins and Complexes up to m/Z=1,000,000. *Abstracts of Papers of the American Chemical Society* **2012**, *244*.

(10) Wang, X.; Chen, H.; Lee, J.; Reilly, P. T. A. Increasing the Trapping Mass Range to m/Z=10(9)-A Major Step toward High Resolution Mass Analysis of Intact RNA, DNA and Viruses. *International Journal of Mass Spectrometry* **2012**, *328*, 28–35. https://doi.org/10.1016/j.ijms.2012.07.024.

(11) Lee, J.; Chen, H.; Liu, T.; Berkman, C. E.; Reilly, P. T. A. High Resolution Time-of-Flight Mass Analysis of the Entire Range of Intact Singly-Charged Proteins. *Analytical Chemistry* **2011**, *83*, 9406–9412. https://doi.org/10.1021/ac202001z.

(12) Schrader, R. L.; Walker, T. E.; Chakravorty, S.; Anderson, G. A.; Reilly, P. T. A.; Russell, D. H. Optimization of a Digital Mass Filter for the Isolation of Intact Protein Complexes in Stability Zone 1,1. *Analytical Chemistry* **2023**, *95* (5), 3062–3068. https://doi.org/10.1021/acs.analchem.2c05221.

(13) McCabe, J. W.; Jones, B. J.; Walker, T. E.; Schrader, R. L.; Huntley, A. P.; Lyu, J.; Hoffman, N. M.; Anderson, G. A.; Reilly, P. T. A.; Laganowsky, A.; Wysocki, V. H.; Russell, D. H. Implementing Digital-Waveform Technology for Extended m/z Range Operation on a Native Dual-Quadrupole FT-IM-Orbitrap Mass Spectrometer. *Journal of the American Society for Mass Spectrometry* **2021**, *32* (12), 2812–2820. https://doi.org/10.1021/jasms.1c00245.

(14) Lantz, C.; Schrader, R.; Meeuwsen, J.; Shaw, J.; Goldberg, N. T.; Tichy, S.; Beckman, J.; Russell, D. H. Digital Quadrupole Isolation and Electron Capture Dissociation on an Extended Mass Range Q-TOF Provides Sequence and Structure Information on Proteins and Protein Complexes. *J. Am. Soc. Mass Spectrom.* **2023**, *34* (8), 1753–1760. https://doi.org/10.1021/jasms.3c00184.

(15) Brabeck, G. F.; Reilly, P. T. A. Ion Manipulation by Digital Waveform Technology. *Special Issues* **2015**, *13* (2), 34–44.

(16) Reece, M. E.; Huntley, A. P.; Moon, A. M.; Reilly, P. T. A. Digital Mass Analysis in a Linear Ion Trap without Auxiliary Waveforms. *Journal of the American Society for Mass Spectrometry* **2020**, *31* (1), 103–108. https://doi.org/10.1021/jasms.9b00012.

(17) Huntley, A. P.; Reilly, P. T. A. Computational Evaluation of a New Digital Tandem Quadrupole Mass Filter. *Journal of Mass Spectrometry* **2021**, *56* (2), e4699. https://doi.org/10.1002/jms.4699.

(18) Huntley, A. P.; Reilly, P. T. A. On the Relationships between Resolution, Dimensionless Stability, Pseudopotential Well Depth, Acceptance, and Transmission in Mass Filters. *J Mass Spectrom* **2022**, *57* (4), e4825. https://doi.org/10.1002/jms.4825.

(19) Huntley, A. P.; Brabeck, G. F.; Reilly, P. T. A. Influence of the RF Drive Potential on the Acceptance Behavior of Pure Quadrupole Mass Filters Operated in Stability Zones A and B. *Int J Mass Spectrom* **2020**, *450*, 116303. https://doi.org/10.1016/j.ijms.2020.116303.

(20) Reilly, P. T. A.; Chakravorty, S.; Bailey, C. F.; Obe, F. O.; Huntley, A. P. Will the Digital Mass Filter Be the Next High-Resolution High-Mass Analyzer? *Journal of the American Society for Mass Spectrometry* **2021**, *32* (10), 2615–2620. https://doi.org/10.1021/jasms.1c00234.

(21) Chakravorty, S.; Obe, F. O.; Groetsema, E.; Reilly, P. T. A. Effect of Jitter on Digital Mass Filter Analysis in Higher Stability Zones. *Journal of the American Society for Mass Spectrometry* **2022**. https://doi.org/10.1021/jasms.2c00293.

(22) Obe, F. O.; Chakravorty, S.; Groetsema, E.; Collings, B. A.; Hager, J. W.; Reilly, P. T. A. Experimental Validation of the Digital Tandem Mass Filter. *J Am Soc Mass Spectrom* **2023**, *34* (2), 154–160. https://doi.org/10.1021/jasms.2c00234.

(23) Du, Z.; J. Douglas, D.; Konenkov, N. Elemental Analysis with Quadrupole Mass Filters Operated in Higher Stability Regions. *Journal of Analytical Atomic Spectrometry* **1999**, *14* (8), 1111–1119. https://doi.org/10.1039/A804022B.

(24) Du, Z.; Douglas, D. J. A Novel Tandem Quadrupole Mass Analyzer. *Journal of the American Society for Mass Spectrometry* **1999**, *10* (11), 1053–1066. https://doi.org/10.1016/S1044-0305(99)00094-X.

(25) Chen, W.; Collings, B. A.; Douglas, D. J. High-Resolution Mass Spectrometry with a Quadrupole Operated in the Fourth Stability Region. *Anal Chem* **2000**, *72* (3), 540–545. https://doi.org/10.1021/ac990815u.

(26) Dawson, P. H. The Acceptance of the Quadrupole Mass Filter. *International Journal of Mass Spectrometry and Ion Physics* **1975**, *17*, 423–445.

(27) Dawson, P. H. Fringing Fields in the Quadrupole Mass Filter. *International Journal of Mass Spectrometry and Ion Physics* **1971**, *6* (1), 33–44. https://doi.org/10.1016/0020-7381(71)83002-4.

(28) Dawson, P. H.; Bingqi, Y. The Second Stability Region of the Quadrupole Mass Filter. I. Ion Optical Properties. *International Journal of Mass Spectrometry and Ion Processes* **1984**, *56* (1), 25–39. https://doi.org/10.1016/0168-1176(84)85076-4.

(29) Dawson, P. H.; Bingqi, Y. The Second Stability Region of the Quadrupole Mass Filter. II. Experimental Results. *International Journal of Mass Spectrometry and Ion Processes* **1984**, *56* (1), 41–50. https://doi.org/10.1016/0168-1176(84)85077-6.

(30) March, R. E.; Todd, J. F. J. *Quadrupole Ion Trap Mass Spectrometry*; J. Wiley: Hoboken, N.J., 2005.

(31) *Quadrupole Mass Spectrometry and Its Applications*; Dawson, P. H., Ed.; Dylla, H. F., Series Ed.; AVS Classics in Vacuum Science and Technology; AIP Press: Woodbury, NY, 1995.

(32) Brabeck, G. F.; Reilly, P. T. A. Mapping Ion Stability in Digitally Driven Ion Traps and Guides. *Int J Mass Spectrom* **2014**, *364*, 1–8. https://doi.org/10.1016/j.ijms.2014.03.008.

(33) Brabeck, G. F.; Wang, L.; Reilly, P. T. A. Development of High-Precision Digital Waveform Generator to Enable next Generation Digital Ion Traps and Guides; St Louis, MO, 2015.

(34) Hoffman, N. M.; Gotlib, Z. P.; Opačić, B.; Clowers, B. H.; Reilly, P. T. A. Generation of Digital Waveforms with High Resolution Duty Cycle; Indianapolis, IN, 2017.

(35) Huntley, A. P.; Reilly, P. T. A. Computational Evaluation of Mass Filter Acceptance and Transmittance Influenced by Developing Fields: An Application of the Plane Method to Investigate Prefilter Efficacy for Rectangular Wave Operated Mass Filters. *J Mass Spectrom* **2020**, *55* (6), e4510. https://doi.org/10.1002/jms.4510.

(36) Huntley, A. P.; Brabeck, G. F.; Reilly, P. T. A. Tutorial and Comprehensive Computational Study of Acceptance and Transmission of Sinusoidal and Digital Ion Guides. *J Mass Spectrom* **2019**, *54* (11), 857–868. https://doi.org/10.1002/jms.4440.

(37) Brubaker, W. M. An Improved Quadrupole Mass Analyzer. *Adv. Mass Spectrom* **1968**, *4*, 293–299.

(38) Konenkov, N. V.; Sudakov, M.; Douglas, D. J. Matrix Methods for the Calculation of Stability Diagrams in Quadrupole Mass Spectrometry. *J. Am. Soc. Mass Spectrom.* **2002**, *13* (6), 597–613. https://doi.org/10.1016/S1044-0305(02)00365-3.

TOC Figure: